JCTC Journal of Chemical Theory and Computation

Simulating POPC and POPC/POPG Bilayers: Conserved Packing and Altered Surface Reactivity

Lorant Janosi and Alemayehu A. Gorfe*

Department of Integrative Biology and Pharmacology, University of Texas Health Science Center at Houston, 6431 Fannin Street, MSB 4.108, Houston, Texas 77030

Received July 8, 2010

Abstract: Molecular dynamics (MD) simulation is a popular technique to study bilayer structural properties, but it has not been widely used in mixed bilayers of neutral and charged lipids. Here, we present results from constant temperature and pressure MD simulations of a 2-oleoyl-1-pamlitoyl-*sn*-glyecro-3-phosphocholine (POPC) bilayer containing 23% 2-oleoyl-1-pamlitoyl-*sn*-glyecro-3-glycerol (POPG). The simulations were performed using the recently updated CHARMM force field and involved two bilayers of 104 and 416 lipids. A control simulation of a pure POPC bilayer of 128 lipids yielded equilibrium structural properties that compare very well with experimental data. The average equilibrium properties of the mixed bilayer systems were very similar to those of the pure POPC. However, nearly one-half of all the POPG lipids were found to be involved in hydrogen bonding with POPC lipids. Furthermore, the hydration of the mixed bilayer is different from that of the pure POPC, with the former inducing ordering of water molecules at longer distances. Thus, a phospholipid bilayer with ~23% negative charge content in the liquid crystalline phase differs from its neutral counterpart only at the headgroup.

1. Introduction

Many cytosolic proteins that have a cluster of basic residues or a polycationic domain, such as the signaling mediator K-ras, bind to the negatively charged inner leaflet of the plasma membrane.[1] The mechanism by which these proteins target the host bilayer continues to be a subject of intense experimental scrutiny.[2] Computational approaches, such as molecular dynamics simulation (MD), play key roles in the study of pure bilayers with and without bound proteins and peptides.[3,4] They complement the experimental efforts by characterizing the atomic interactions responsible for the protein−membrane recognition.[3,5] However, such an MD study requires constructing a well-equilibrated bilayer system containing the right balance of neutral and charged phospholipids. On the basis of data from fully equilibrated MD simulations, this work describes the structural and dynamic behaviors of a mixture of 2-oleoyl-1-pamlitoyl-*sn*-glyecro-3-phosphocholine (POPC) and 2-oleoyl-1-pamlitoyl-*sn*-glyecro-3-glycerol (POPG) lipid bilayer (Figure 1).

A number of MD studies targeted the POPC bilayer using several different force fields (FFs), including AMBER,[6] CHARMM,[7,8] GROMOS,[9] and others.[10] The ensemble-averaged bilayer properties derived from these simulations were in overall agreement with each other and with experimental data. However, there were discrepancies too, particularly in the characterization of the lateral organization of the bilayers by the area per lipid (A_L), which varied between 63.8 and 69.3 Å^2 in the simulations.[11] Interestingly, the A_L from experiments also varied between 63.0 and 68.3 Å^2.[12−15] Both the simulations (298−303 K) and the experiments (297−310 K) were done at temperatures well above the gel−liquid crystalline (L_α) phase transition temperature of 268 K.[16] Such ambiguity in the experimental A_L presented a particular challenge for the fully atomistic CHARMM27 (C27) FF,[17] which best preserves bilayer properties for simulations under constant area or surface tension condition.[18,19] A number of improvements[20−22] have been made to mitigate the dramatic lateral contraction that occurs during an isothermal isobaric, that is, constant temperature and pressure (NPT) simulation with C27. The improvements ranged from updating only the acyl chain torsions,[20,21] to reparametrizing

* Corresponding author phone: (713) 500-7538; fax: (713) 500-7444; e-mail: alemayehu.g.abebe@uth.tmc.edu.

10.1021/ct100381g
Published on Web 09/24/2010

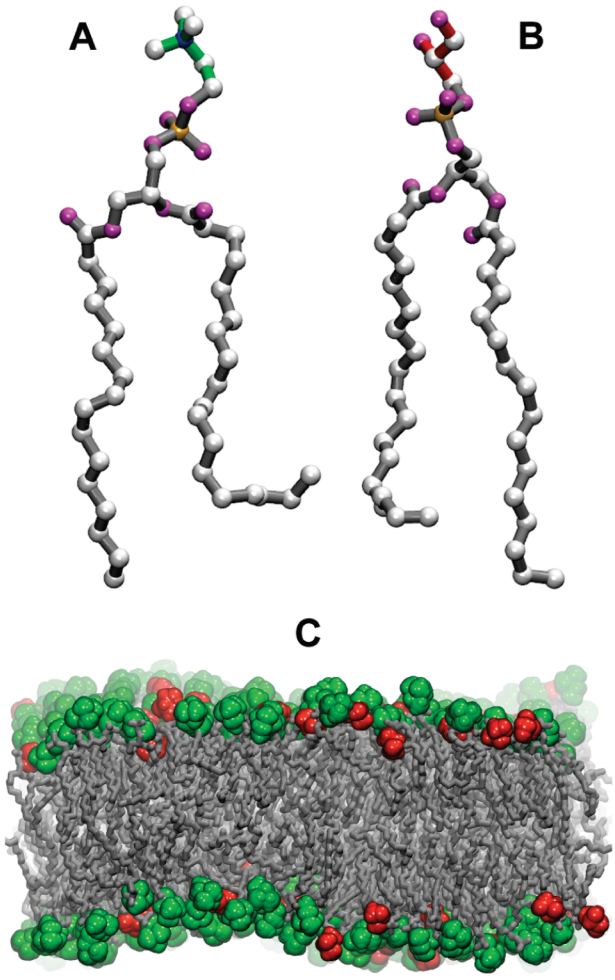

Figure 1. The structure of the POPC (A) and POPG (B) lipids represented by ball-and-stick models, with bonds at the headgroup colored green (choline) and red (glycerol), whereas carbon is in white, oxygen is in purple, nitrogen is in blue, and phosphorus is in tan. (C) A snapshot from the large simulation (SIIb, see Table 1) of the mixed bilayer containing 320 POPC (green) and 96 POPG (red) lipids. Water molecules, ions, and hydrogen atoms were omitted for clarity.

charges on the headgroup and upper chain atoms,[22] to modification of selected torsional, Lennard-Jones, and partial atomic charge parameters.[23] The latter has been incorporated into the new CHARMM36 (C36) parameter set and was tested with six lipids (including POPC). In all cases, it yielded bilayer structural properties that are in very good agreement with experiments.[23]

In the current work, the C36 FF was used to perform tensionless NPT simulations of pure POPC and a POPC/POPG mixture. The POPC/POPG bilayer was simulated in two system sizes: a small system of 104 lipids and a large one of 416 lipids. In both cases, we found that ~75% of all the POPG molecules are engaged in intra- or intermolecular hydrogen bonding, in agreement with several previous reports on the strong propensity of POPG lipids to form hydrogen bonds.[6,24,25] The pure POPC simulation also yielded results that are consistent with experimental data. The simulations predict that bilayers of POPC without and with 23% POPG have nearly identical equilibrium structural properties, including area per lipid, bilayer thickness, and area compressibility modulus.

2. Methods

Three MD simulations, a pure POPC bilayer (simulation SI), a small POPC/POPG bilayer (SIIa), and a large POPC/POPG bilayer (SIIb), were carried out in the NPT ensemble at $T = 310$ K and $P = 1.01325$ atm (Table 1). The simulations used the C36 FF and were run with the NAMD program.[26] Visualization and some of the analyses were carried out with VMD.[27]

The initial model for the pure POPC bilayer (SI) was built using the CHARMM GUI bilayer builder[28,29] and consisted of 128 lipids (64 per leaflet) solvated by 6052 water molecules in a box of $67.1 \times 67.1 \times 76.1$ Å^3. The starting point for the small POPC/POPG bilayer (SIIa) was originally constructed as pure POPC bilayer of 104 lipids. After a short minimization and equilibration (see below), 24 POPC lipids were randomly selected and replaced by POPG lipids, resulting in a system of 52 lipids per leaflet (40 POPC and 12 POPG) solvated by 6224 water molecules in a box of $58.7 \times 58.7 \times 96.0$ Å^3. Twenty-four sodium ions were added to neutralize the total charge of the system. After SIIa was run for 70 ns, a snapshot was taken and multiplied into four copies, which were then assembled into a large bilayer consisting of 320 POPC and 96 POPG lipids (a total of 130 096 atoms).

Each system was minimized for 2000 steps with all nonhydrogen atoms fixed and for another 2000 steps with only the phosphorus atoms harmonically restrained ($k = 4$ kcal mol^{-1} Å^{-2}). This was followed by 200 ps equilibration, and by another 300 ps equilibration with k scaled by 0.75, 0.5, and 0.25 every 100 ps. A single production simulation for each system was then run for the durations listed in Table 1. The integration time step, δt, was 1 fs during the equilibration runs. For the production phase, $\delta t = 2$ fs was used in conjunction with constraints applied to all bonds involving hydrogens using the SHAKE algorithm.[30] The NAMD multi-timestepping procedure was used with the bonded and nonbonded forces computed at every δt and the particle mesh Ewald (PME) calculations at every $2\delta t$; the step cycle was 10. The cutoffs for nonbonded interactions and for pair-list updates were 12 and 14 Å, respectively, with the switch function turned on at 10 Å.

3. Results and Discussion

In the following sections, we first examine the performance of the C36 FF and then describe the structure and dynamics of the POPC bilayer in the presence and absence of POPG lipids.

3.1. Performance of C36 Relative to C27. Membrane simulation with C27 FF works best when the area is fixed (see Introduction), which can be done for pure bilayers of the common lipids whose A_L is well-documented (e.g., DMPC and DPPC). Constant area simulation becomes problematic when unambiguous A_L is not available or when the lateral dimensions of the simulation box must change during the simulation. The former is typically true for

Table 1. Simulations Performed and Bilayer Structural Properties (Average ± S.D.)[a]

sim.	composition	no. of lipids (atoms)	length (ns)	A_L (Å^2) exp./prev. sim.[b]	K_A (mN/m) exp./ prev. sim.[c]	D_{P-P} (Å) exp./ prev. sim.[d]	D_{C2-C2} (Å)
SI	POPC	128 (35 340)	75	64.7 ± 1.3 54,[13] 63,[15] 68.3,[12] 66[14]/65.5,[7] 63.8,[11] 66.8,[10] 63.5[6]	272 180−330[34]/ 404[11]	39.1 ± 0.6 37[12]/ 34.6,[11] 35.5[6]	28.2 ± 0.6
SIIa	POPC/POPG	104 (32 524)	70	63.6 ± 1.2	346	39.7 ± 0.6	28.7 ± 0.5
SIIb	POPC/POPG	416 (130 096)	120	64.4 ± 0.8	295 ± 74 (238)	39.1 ± 0.4	28.2 ± 0.3

[a] The first 20 ns of the data from each trajectory was excluded from the analyses. D_{P-P} represents bilayer thickness, measured as the average distance along the membrane normal between the centers of mass of the phosphorus atoms of the two leaflets; A_L is the area per lipid, measured as the average area of the simulation box (obtained from its lateral dimensions) normalized by the number of lipids per leaflet; K_A is the area compressibility modulus at constant temperature, calculated as in eq 1 over the last 50 ns (and over the last 100 ns in parentheses for SIIb); and D_{C2-C2} represents the hydrophobic thickness, measured as the average distance along the membrane normal between the centers of mass of the first methyl carbon atoms of the two leaflets. [b] Experiments at 275 K,[13] 297 K,[15] 303 K,[12] and 310 K;[14] simulations at 300 K,[7] 303 K,[11] 303 K,[10] and 310 K.[6] [c] Simulation at 303 K.[11] [d] Experiment at 303 K;[12] simulations at 303 K[11] and 310 K.[6] The current simulations were carried out at 310 K.

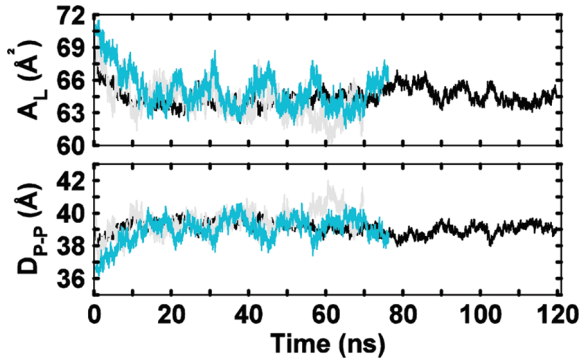

Figure 2. Time evolution of the area per lipid (A_L) and bilayer thickness (D_{P-P}) in the pure POPC (SI, cyan) simulation, and small (SIIa, light gray) and large (SIIb, black) POPC/POPG bilayer simulations.

multicomponent bilayers. The latter occurs during insertion of a molecule of non-negligible size into small bilayer patches. In the current work, we used the C36 FF that allowed us to run NPT simulations in which the system is able to adjust its area to minimize unfavorable atomic contacts. For comparison, we performed a 60 ns NPT simulation with the C27 FF using a copy of the system in SIIa. Figure S1 plots the time evolution of the bilayer thickness (D_{P-P}) from this simulation, which can be compared to the corresponding plot in Figure 2 obtained from simulation SIIa (i.e., performed with the C36 FF). The continuous compaction (or thickening) of the bilayer in Figure S1 relative to the equilibration achieved in Figure 2 clearly shows that NPT simulation with C27 yields unacceptable results. In contrast, the simulations with C36 produced results that are in very good agreement with available experimental data (Table 1).

3.2. Bilayer Structural Properties. *3.2.1. Pure POPC.* The time evolution of the bilayer thickness, D_{P-P}, and area per lipid, A_L, in the pure POPC simulation (Figure 2, cyan) shows that the bilayer has equilibrated after approximately 20 ns. The symmetric number density distributions along the bilayer normal, z, calculated for various components of POPC (Figure 3) are also consistent with a well-equilibrated bilayer system. The distributions further indicate that water penetrates the bilayer up to the glycerol-ester region, while the methyl groups of the lipid tails are fully dehydrated, in agreement with experiments.[12,31,32] Furthermore, the ensemble-averaged D_{P-P}, A_L, and D_{C2-C2} (hydrophobic thickness) of

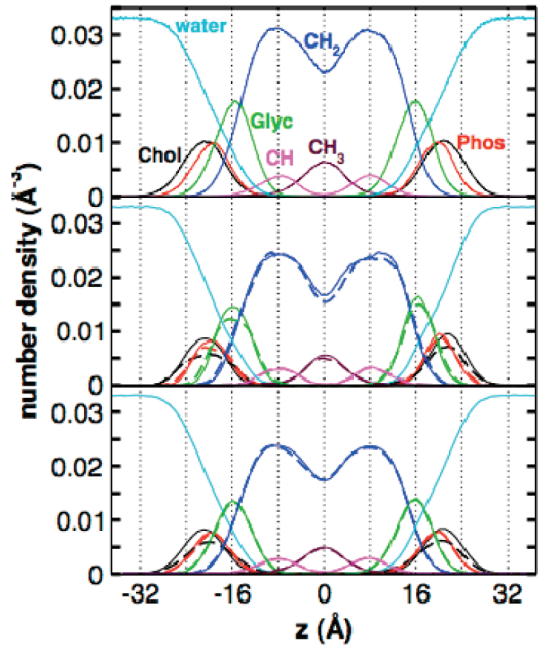

Figure 3. Number density distributions for the various components of POPC (solid lines) and POPG (dashed lines) lipid derived from simulation SI (top panel), SIIa (middle panel), and SIIb (bottom panel). In this and subsequent figures, only the equilibrated portions of the trajectories were used, that is, excluding the first 20 ns. All the groups (labeled in the top panel) contain their heavy atoms only. The dashed black line in the two bottom panels corresponds to the glycerol headgroup of the POPG lipid. The number densities for POPG were rescaled by a factor that matches the CH_2 profiles to those of POPC.

the POPC bilayer agree well with results from previous simulations and experiments (Table 1). For example, Rog et al.[6] and Poger et al.[11] reported A_L values of 63.5 and 63.8 Å^2 from simulations with the AMBER94[33] FF and an improved version of the GROMOS96 FF, respectively. Our A_L of 64.6 Å^2 is close to these values, as well as to the experimental data reported by Smaby et al. (63 Å^2[15]) and Hyslop et al. (66 Å^2[14]). However, the current A_L is somewhat smaller than the 68.3 Å^2 obtained by Kucerka et al.[12] The difficulty associated with the lack of unambiguous experimental data, particularly for A_L, has been discussed in a recent work that systematically compared various structural parameters from MD and experiments.[11]

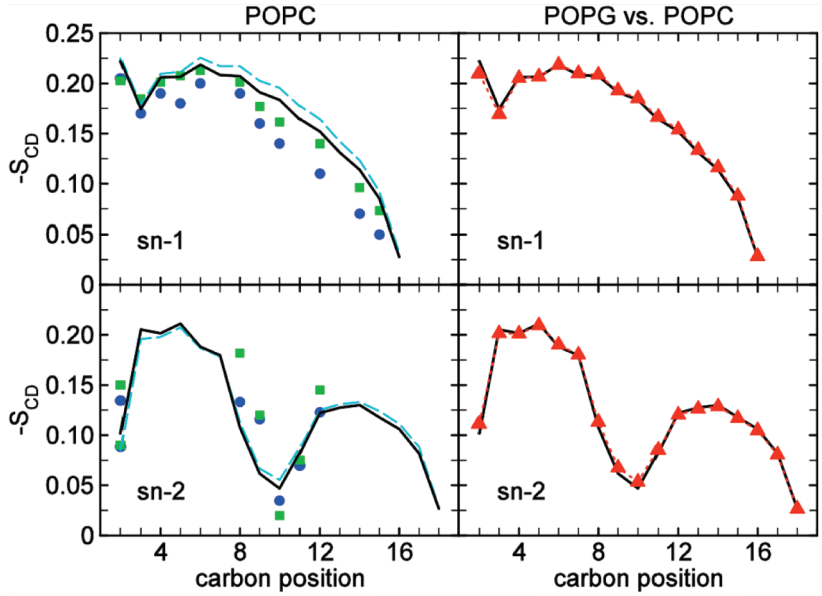

Figure 4. Deuterium order parameter ($-S_{CD}$) profiles. Left column shows a comparison between POPC order parameters (sn-1, top and sn-2, bottom) obtained from the pure POPC system (dashed line), the large POPC/POPG (black solid line), and experimental data at 300 K (■) and 315 K (●) from Seelig and colleagues.[16,41] The column on the right compares profiles for POPG sn-1 and sn-2 tails (symbols) with those for POPC (lines) extracted from SIIb.

Fluctuation in A_L at constant temperature is related to an important bilayer property, the isothermal area compressibility modulus, K_A, given by

$$K_A = \frac{2k_B\langle T\rangle\langle A_L\rangle}{N_L\sigma^2} \quad (1)$$

where k_B is the Boltzmann constant, σ^2 is the variance associated with A_L, N_L is the number of lipids, and the angle brackets denote time and ensemble averages. The large fluctuations in the area (Figure 2) resulted in large variance, σ^2, leading to $K_A = 272$ mN m^{-1} (Table 1), which falls within the experimental range of 180−330 mN m^{-1}.[34]

The behavior of the hydrocarbon tails was examined using the deuterium order parameter, S_{CD}, calculated from the trajectory as

$$S_{CD} = \frac{1}{2}\langle 3\cos^2\theta - 1\rangle \quad (2)$$

where θ is the angle between a C−H bond of the methylene/methyl group in a given acyl chain and the bilayer normal. Overall, the calculated S_{CD} values are in very good agreement with the experimental data (Figure 4), particularly at the often poorly predicted chain termini. The agreement with experiment is best for the sn-2 chain, whereas the S_{CD}'s associated with carbons in the middle of the sn-1 chain are slightly overestimated. These results are consistent with those reported by Klauda et al. in their evaluation of the C36 force field.[23] In so far as S_{CD} partly measures chain ordering, and given the connection between chain order and membrane thickness, it is safe to assume that the somewhat high D_{P-P} may be due to the enhanced ordering of the saturated sn-1 tail. This could be an area for additional improvements in future updates of the FF.

3.2.2. POPC/POPG Mixed Bilayer. Global Structure. The structural properties of the small POPC/POPG bilayer derived from simulation SIIa are surprisingly close to those of the pure POPC bilayer of comparable size (Table 1, Figures 2 and 3). Both the instantaneous (Figure 2) and the ensemble-averaged (Table 1) values of A_L, D_{P-P}, and D_{C2-C2} are nearly identical in the two simulations. The K_A calculated from SIIa is also fairly close to that from the pure POPC bilayer simulation (Table 1). The number density distributions for POPC and POPG in the binary mixture are also very similar to each other and to those of the pure POPC bilayer (Figure 3, top and middle panels). Minor differences are present only between the distributions of the glycero-ester oxygen atoms of the two leaflets in SIIa (Figure 3). However, the position of the peaks did not change when the distributions were computed using the last 10, 20, 30, and 40 ns data (not shown), indicating that the equilibrium structural properties discussed above remain valid.

To ensure that these results are not artifacts due to the small size of the binary mixture, we simulated a larger system for a longer duration under identical simulation conditions (see Methods). Comparison of the results from this simulation (SIIb) with those of the pure POPC or the smaller POPC/POPG (SIIa) trajectories (Table 1, Figures 2 and 3) clearly shows that the calculated averages from each of the three trajectories are within error of each other. The only noticeable differences are in the symmetry of the distributions for the glycero-ester oxygens (Figure 3, lower panel) and in the amplitude of the fluctuations in A_L and D_{P-P} (Figure 2, see also the SD in Table 1). The large simulation yielded perfectly symmetric distributions and smaller fluctuations due perhaps to the improved statistics afforded by the increased number of lipids and longer simulation time. The change in fluctuation has a direct impact on K_A (see eq 1), so that the obtained K_A from SIIb became closer to that from the pure

POPC bilayer (Table 1). Thus, in the following sections, we will use the larger system (SIIb) to characterize the POPC/POPG bilayer structure and dynamics in more detail.

In the past, several NPT MD simulation studies have been done on the negatively charged POPG in the pure form[24,25] or mixed with POPE,[6] but to our knowledge none in its mixture with POPC. Comparing the current results with those studies is nevertheless instructive. By analyzing POPC and POPE/POPG trajectories, Rog et al.[6] obtained very similar area and thickness for POPC (A_L = 63.5 Å^2 and D_{P-P} = 35.6 Å) and POPG (A_L = 62.8 Å^2 and D_{P-P} = 35.5 Å) lipids. On the other hand, Elmore[25] calculated A_L(POPG) = 56.1 Å^2 and A_L(POPC) = 68.4 Å^2 based on 50 and 10 ns trajectories of pure POPG and POPC bilayers, respectively. In the case of the POPC bilayer, the discrepancy between our and Elmore's results may be explained by the different lengths of the simulations, because we were able to reproduce their data from the first 10 ns of our trajectory (not shown). We would like to note that parameters used by Elmore for POPG were taken from the PRODRG server,[35,36] which does not give a rigorous, consistent set of parameters. Despite the lack of experimental data to validate a PG force field, the CHARMM parameter set for PGs is consistent with the general CHARMM force field for biomolecules (in terms of bonded terms, van der Waals terms, and charges). Therefore, it would not be surprising if Elmore's parameters showed some discrepancy. However, a more recent study[24] based on much longer simulations of pure POPG and POPC reported A_L(POPG) = 53.0 Å^2 and A_L(POPC) = 65.8 Å^2. Although differences in length, force field, and composition among these simulations preclude a direct comparison, the large variations in these results suggest that more work is required to determine the structural properties of POPG in the pure form and in its mixture with other lipids. Our results suggest that the global structural properties of a POPC bilayer containing 23% POPG are very similar to those of the pure POPC bilayer.

Chain Order and Dynamics. Because POPC and POPG lipids differ only at the headgroup, where choline ($-CH_2-CH_2-N^+-(CH_3)_3$) of the former is replaced by glycerol ($-CH_2-[(CH)(OH)]-CH_2-OH$) in the latter, we wanted to know if the nearly identical average A_L, D_{P-P}, and D_{C2-C2} discussed above are a consequence of similar packing and dynamics of the identical hydrophobic tails of the two lipid types. Thus, we compared the POPC and POPG lipid tails using the deuterium order parameter, S_{CD}, and the rotational autocorrelation function. The S_{CD} profiles for the POPC tails in the binary mixture show ordering similar to that of the pure bilayer and are almost identical to the POPG ones (Figure 4). The lateral diffusion coefficients, D, calculated from the slope of the mean square displacement of individual lipids (see Figure S2) and averaged over the number of the POPC and POPG lipids are also within error of one another. In the pure phase, $D_{POPC} \approx 8.9 \pm 0.7 \times 10^{-8}$ cm^2/s (error estimated by block averaging, see Supporting Information), which compares very well with the experimental data for the fully hydrated POPC bilayer at 313 K, $\sim 14 \times 10^{-8}$ cm^2/s,[37] and at 322 K, $\sim 19 \times 10^{-8}$ cm^2/s,[38] as well as with results from previous simulations (e.g., 6.5×10^{-8} cm^2/s[39]).

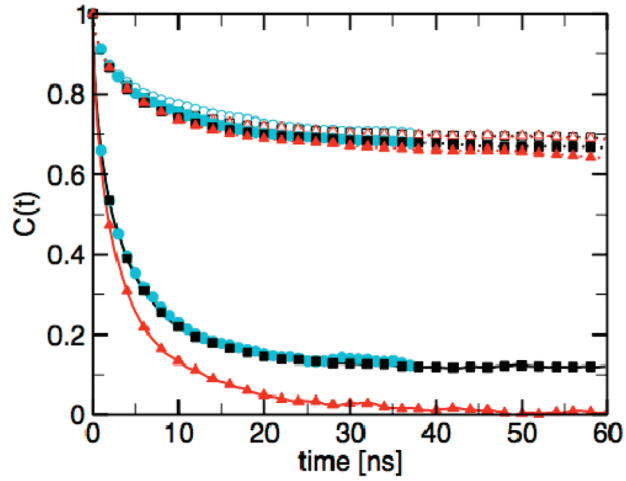

Figure 5. First rank rotational autocorrelation functions calculated for the headgroups (solid lines) and hydrophobic tails (dotted lines, sn-1, empty symbols; sn-2, filled symbols) for POPC in the pure (circles) and mixed (squares) bilayer, and for POPG in the mixed bilayer (triangles). The autocorrelation functions are computed for the headgroups using vectors P→N (C_{12} for POPG − central carbon of the glycerol headgroup) and the tails using the vector between the first ethyl and the terminal methylene carbon atoms.

In the binary mixture, we obtained $D_{POPC} \approx 9.1 \pm 0.6 \times 10^{-8}$ cm^2/s and $D_{POPG} \approx 9.2 \pm 0.5 \times 10^{-8}$ cm^2/s.

The average rotational autocorrelation functions, calculated for each tail and for the headgroups, are shown in Figure 5. In contrast to the clear differences in the fast-relaxing headgroups, where the two lipids are chemically different, the POPC and POPG tails exhibit nearly identical rotational behavior. The rotational autocorrelation functions for the sn-1 tails overlap, while those of the sn-2 tails of POPG decorrelate slightly faster than for POPC. We conclude that the lipid tails of POPC and POPG in a mixture behave in the same manner as the pure POPC tails. As a consequence, the bilayer thickness, area per lipid, and other structural quantities that are predominantly dictated by lipid packing at the L_α phase remain unaffected. The effect of the POPG lipids is thus limited to the lipid−water interfacial region.

Lipid−Lipid Interaction. Previous studies of POPG and POPE/POPG bilayers have found that POPG molecules have a high propensity to form intra-POPG or interlipid hydrogen bonds.[24,25] Thus, we monitored intra- and intermolecular hydrogen bonds using donor−acceptor distance and angle cutoffs of 3.1 Å and 150°. The distributions of the mean number of hydrogen bonds formed per molecule of POPG and POPC are shown in Figure 6A. The histograms show that about 30% of the POPG lipids are engaged in POPG−POPG hydrogen bonding. This interaction is almost exclusively intramolecular, where the hydroxyl headgroup donates a hydrogen to a phosphate (and to some extent the glycero-ester) oxygen atom. Another 45% of the POPG molecules are involved in hydrogen bonding with POPC lipids. Therefore, 75% of all the POPG lipids are engaged in hydrogen bonding. In contrast, an insignificant number of POPC−POPC hydrogen bonds were detected. An important conclusion from these data is the following. Negatively

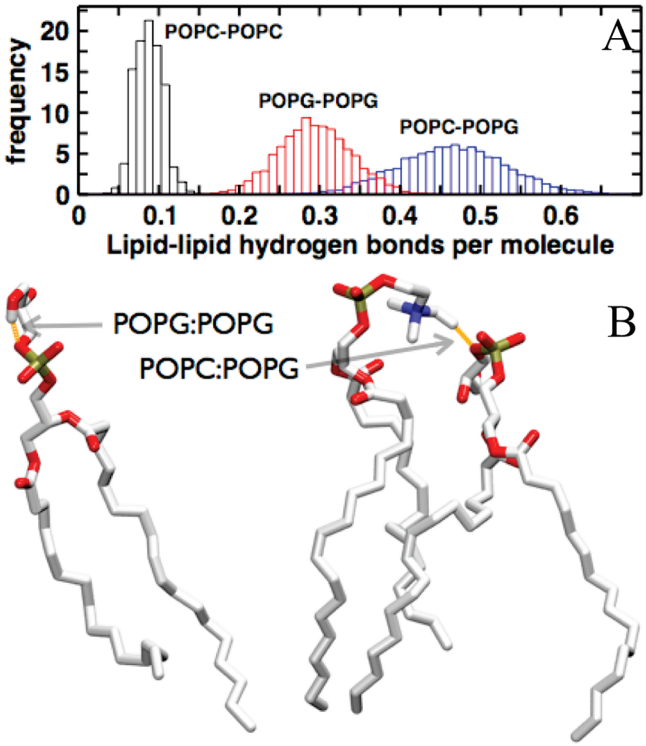

Figure 6. Lipid−lipid hydrogen bonds in the large POPC/POPG bilayer. (A) Histograms showing the frequency distributions for the fraction of POPC molecules involved in hydrogen bonding with other POPC molecules (black), as well as the fraction of POPG molecules involved in intramolecular (red), and in intermolecular hydrogen bonds with POPC (blue). (B) Examples of the intramolecular POPG and interlipid POPC−POPG hydrogen bonds. Hydrogen bonds were defined by a donor−acceptor distance cutoff of 3.1 Å and donor−hydrogen−acceptor angle cutoff of 150°.

charged lipids with the same fatty acid chains as the predominant lipid in the host bilayer preserve the overall structure of the bilayer while inducing a drastically different surface reactivity. These conditions are potentially important for polycationic proteins that preferentially target membrane patches of regular thickness and mechanical property, unlike proteins that target ordered membrane domains or lipid rafts.

Hydration. It is well-known that the phosphate oxygens of lipids polarize the surrounding water molecules in part through the formation of hydrogen bonds.[40] As a result, the average water dipole moment is directed toward the center of the membrane, resulting in a preferred orientation, or ordering, of the interfacial water molecules. To check if the hydration of the mixed bilayer differs from that of the pure POPC, we computed the orientational order parameter of the water molecules in both systems as the average cosine of the angle between the O−H bond and the bilayer normal. The results are plotted in Figure 7 as a function of the water molecules' distance from the membrane center. Water is most ordered around 20 Å, which is the average position of the phosphate group for both the pure POPC and the POPC/POPG bilayers (see Figure 3 and Table 1). As the distance to the bilayer surface increases, the ordering of the water molecules disappears quickly (∼26 Å) for the pure POPC membrane. However, the average ordering of the water around the binary mixture is decreasing very slowly and

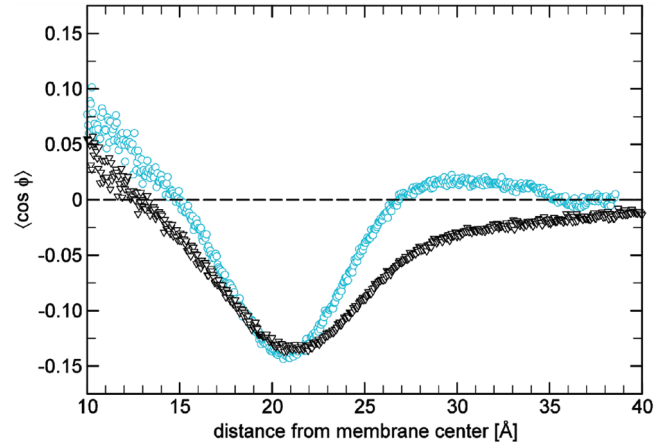

Figure 7. Rank one order parameter of water molecules as a function of distance from the center of the membrane in the pure POPC (○) and large POPC/POPG (▽) bilayers.

vanishes at about 40 Å. This is in qualitative agreement with previous simulations that have shown that pure POPG bilayers induce long-range ordering of water molecules around the bilayer due both to their net negative charge and to the polar hydroxyl oxygens of their glycerol headgroup.[24] Consistent with the conservation of the bilayer structure, the number of hydration water molecules per lipid is similar in the pure POPC bilayer and the binary mixture (see Supporting Information). These results support the conclusions of the previous paragraph that the charged POPG increases the surface reactivity, leading to interlipid interactions and enhanced polarization of the surrounding solvent without affecting the overall structure of the bilayer.

4. Conclusion

In this Article, we presented results from MD simulations of bilayers made up of pure POPC and a binary mixture of POPC lipids containing 23% anionic POPG lipids. The simulations were carried out in the NPT ensemble using the C36 force field. The obtained results for the pure POPC are in very good agreement with experimental data, validating the new C36 force field. The average structural properties of the binary mixture, such as area per lipid, bilayer thickness, and isothermal area compressibility modulus, remain nearly the same as for the pure POPC bilayer. Furthermore, deuterium order parameters for the tails of both POPC and POPG lipids of the binary mixture maintain their values from the pure POPC bilayer. Nonetheless, considerable differences were observed in the behavior of the headgroups, including the strong hydrogen-bonding potential, both intramolecular and interlipid, of the POPG lipids and the enhanced long-range ordering of water molecules at the hydrophobic−hydrophilic and headgroup−water interfaces of the mixed bilayer.

Supporting Information Available: Additional figures and hydration waters per lipid. This material is available free of charge via the Internet at http://pubs.acs.org.

Acknowledgment. We gratefully acknowledge Dr. J. Klauda (University of Maryland) for making the updated CHARMM36 force available to us before its publication,

the Texas Advanced Computing Center, and the National Center for Supercomputing Applications for computational resources.

References

(1) McLaughlin, S.; Murray, D. *Nature* **2005**, *438*, 605–611.

(2) Yeung, T.; Gilbert, G. E.; Shi, J.; Silvius, J.; Kapus, A.; Grinstein, S. *Science* **2008**, *319*, 210–213.

(3) Lindahl, E.; Sansom, M. S. *Curr. Opin. Struct. Biol.* **2008**, *18*, 425–431.

(4) Gorfe, A. A. *Curr. Med. Chem.* **2010**, *17*, 1–9.

(5) Biggin, P. C.; Bond, P. J. *Methods Mol. Biol.* **2008**, *443*, 147–160.

(6) Rog, T.; Murzyn, K.; Pasenkiewicz-Gierula, M. *Acta Biochim. Pol.* **2003**, *50*, 789–798.

(7) Heller, H.; Schaefer, M.; Schulten, K. *J. Phys. Chem.* **1993**, *97*, 8343–8360.

(8) Li, Z.; Venable, R. M.; Rogers, L. A.; Murray, D.; Pastor, R. W. *Biophys. J.* **2009**, *97*, 155–163.

(9) Poger, D.; Van Gunsteren, W. F.; Mark, A. E. *J. Comput. Chem.* **2010**, *31*, 1117–1125.

(10) Jojart, B.; Martinek, T. A. *J. Comput. Chem.* **2007**, *28*, 2051–2058.

(11) Poger, D.; Mark, A. E. *J. Chem. Theory Comput.* **2010**, *6*, 325–336.

(12) Kucerka, N.; Tristram-Nagle, S.; Nagle, J. F. *J. Membr. Biol.* **2005**, *208*, 193–202.

(13) Pabst, G.; Rappolt, M.; Amenitsch, H.; Laggner, P. *Phys. Rev. E* **2000**, *62*, 4000–4009.

(14) Hyslop, P. A.; Morel, B.; Sauerheber, R. D. *Biochemistry* **1990**, *29*, 1025–1038.

(15) Smaby, J. M.; Momsen, M. M.; Brockman, H. L.; Brown, R. E. *Biophys. J.* **1997**, *73*, 1492–1505.

(16) Seelig, J.; Waespe-Sarcevic, N. *Biochemistry* **1978**, *17*, 3310–3315.

(17) Feller, S. E.; MacKerell, A. D. *J. Phys. Chem. B* **2000**, *104*, 7510–7515.

(18) Jensen, M. O.; Mouritsen, O. G.; Peters, G. H. *Biophys. J.* **2004**, *86*, 3556–3575.

(19) Feller, S. E.; Pastor, R. W. *J. Chem. Phys.* **1999**, *111*, 1281–1287.

(20) Klauda, J. B.; Brooks, B. R.; MacKerell, A. D.; Venable, R. M.; Pastor, R. W. *J. Phys. Chem. B* **2005**, *109*, 5300–5311.

(21) Klauda, J. B.; Pastor, R. W.; Brooks, B. R. *J. Phys. Chem. B* **2005**, *109*, 15684–15686.

(22) Sonne, J.; Jensen, M. O.; Hansen, F. Y.; Hemmingsen, L.; Peters, G. H. *Biophys. J.* **2007**, *92*, 4157–4167.

(23) Klauda, J. B.; Venable, R. M.; Freites, J. A.; O'Connor, J. W.; Tobias, D. J.; Mondragon-Ramirez, C.; Vorobyov, I.; Mackerell, A. D.; Pastor, R. W. *J. Phys. Chem. B* **2010**, *114*, 7830–7843.

(24) Zhao, W.; Rog, T.; Gurtovenko, A. A.; Vattulainen, I.; Karttunen, M. *Biophys. J.* **2007**, *92*, 1114–1124.

(25) Elmore, D. E. *FEBS Lett.* **2006**, *580*, 144–148.

(26) Phillips, J. C.; Braun, R.; Wang, W.; Gumbart, J.; Tajkhorshid, E.; Villa, E.; Chipot, C.; Skeel, R. D.; Kale, L.; Schulten, K. *J. Comput. Chem.* **2005**, *26*, 1781–1802.

(27) Humphrey, W.; Dalke, A.; Schulten, K. *J. Mol. Graphics* **1996**, *14*, 33–38.

(28) Jo, S.; Kim, T.; Im, W. *PLoS One* **2007**, *2*, e880.

(29) Jo, S.; Lim, J. B.; Klauda, J. B.; Im, W. *Biophys. J.* **2009**, *97*, 50–58.

(30) Ryckaert, J. P.; Ciccotti, G.; Berendsen, H. J. C. *J. Comput. Phys.* **1977**, *23*, 327–341.

(31) Kucerka, N.; Liu, Y. F.; Chu, N. J.; Petrache, H. I.; Tristram-Nagle, S. T.; Nagle, J. F. *Biophys. J.* **2005**, *88*, 2626–2637.

(32) Gawrisch, K.; Gaede, H. C.; Mihailescu, M.; White, S. H. *Eur. Biophys. J.* **2007**, *36*, 281.

(33) Wang, J. M.; Wolf, R. M.; Caldwell, J. W.; Kollman, P. A.; Case, D. A. *J. Comput. Chem.* **2004**, *25*, 1157–1174.

(34) Binder, H.; Gawrisch, K. *J. Phys. Chem. B* **2001**, *105*, 12378–12390.

(35) Schuttelkopf, A. W.; van Aalten, D. M. *Acta Crystallogr., Sect. D: Biol. Crystallogr.* **2004**, *60*, 1355–1363.

(36) van Aalten, D. M.; Bywater, R.; Findlay, J. B.; Hendlich, M.; Hooft, R. W.; Vriend, G. *J. Comput.-Aided Mol. Des.* **1996**, *10*, 255–262.

(37) Filippov, A.; Oradd, G.; Lindblom, G. *Biophys. J.* **2003**, *84*, 3079–3086.

(38) Gaede, H. C.; Gawrisch, K. *Biophys. J.* **2003**, *85*, 1734–1740.

(39) Bockmann, R. A.; Hac, A.; Heimburg, T.; Grubmuller, H. *Biophys. J.* **2003**, *85*, 1647–55.

(40) Aman, K.; Lindahl, E.; Edholm, O.; Hakansson, P.; Westlund, P. O. *Biophys. J.* **2003**, *84*, 102–115.

(41) Seelig, A.; Seelig, J. *Biochemistry* **1977**, *16*, 45–50.

CT100381G